*Article*

# Functionalization of Na$_2$Ca$_2$Si$_3$O$_9$/Ca$_8$Si$_5$O$_{18}$ Nanostructures with Chitosan and Terephthalaldehyde Crosslinked Chitosan for Effective Elimination of Pb(II) Ions from Aqueous Media

Eida S. Al-Farraj [1,*], Abdullah N. Alotaibi [1], Ehab A. Abdelrahman [1,2,*], Fawaz A. Saad [3], Khalil ur Rehman [4], Faisal K. Algethami [1] and Reem K. Shah [3]

[1] Department of Chemistry, College of Science, Imam Mohammad Ibn Saud Islamic University (IMSIU), Riyadh 11623, Saudi Arabia
[2] Chemistry Department, Faculty of Science, Benha University, Benha 13518, Egypt
[3] Department of Chemistry, Faculty of Science, Umm Al-Qura University, Makkah 21955, Saudi Arabia; fasaad@uqu.edu.sa (F.A.S.)
[4] Institute of Chemical Sciences, Gomal University, Dera Ismail Khan 29111, KPK, Pakistan
[*] Correspondence: esalfarraj@imamu.edu.sa (E.S.A.-F.); eaaahmed@imamu.edu.sa (E.A.A.)

**Abstract:** Lead poses significant health risks to humans, including neurological and developmental impairments, particularly in children. Additionally, lead pollution in the environment can contaminate soil, water, and air, endangering wildlife and ecosystems. Therefore, this study reports the straightforward fabrication of Na$_2$Ca$_2$Si$_3$O$_9$/Ca$_8$Si$_5$O$_{18}$ nanostructures (NaCaSilicate) utilizing a sol-gel technique. Additionally, the produced nanostructures underwent further modification with chitosan (CS@NaCaSilicate) and chitosan crosslinked with terephthalaldehyde (CCS@NaCaSilicate), resulting in new nanocomposite materials. These samples were developed to efficiently extract Pb(II) ions from aqueous media through complexation and ion exchange mechanisms. Furthermore, the maximum adsorption capacity for Pb(II) ions by the NaCaSilicate, CS@NaCaSilicate, and CCS@NaCaSilicate samples is 185.53, 245.70, and 359.71 mg/g, respectively. The uptake of Pb(II) ions was characterized as spontaneous, exothermic, and chemical, with the best description provided by the Langmuir equilibrium isotherm and the pseudo-second-order kinetic model. Furthermore, a 9 M hydrochloric acid solution effectively eliminated Pb(II) ions from the synthesized samples, attaining a desorption efficacy surpassing 99%. Additionally, the fabricated samples exhibited efficient reusability across five successive cycles of adsorption and desorption for capturing Pb(II) ions.

**Keywords:** chitosan nanocomposites; Na$_2$Ca$_2$Si$_3$O$_9$/Ca$_8$Si$_5$O$_{18}$ nanostructures; removal; Pb(II) ions

## 1. Introduction

Water contamination with heavy metals is a significant environmental and public health concern worldwide [1–3]. Heavy metals are metallic elements that have high atomic weights and can be toxic or harmful to living organisms, even at low concentrations [4]. Mining, metal processing, and manufacturing industries frequently introduce heavy metals into aquatic systems through wastewater discharge or runoff. Also, the use of fertilizers, pesticides, and animal waste contributes to the accumulation of heavy metal ions in soil and water, which can then leach into groundwater or surface water [5]. Exposure to heavy metals through contaminated drinking water or food can have adverse health effects, including neurological disorders, kidney damage, respiratory issues, cardiovascular diseases, and certain types of cancer. Pregnant women, infants, and children are particularly vulnerable to the effects of heavy metal exposure [6,7]. Lead exposure can cause irreversible neurological damage, particularly in children. It can impair cognitive function, decrease IQ, and lead to behavioral problems such as hyperactivity and learning disabilities. Lead exposure during pregnancy can result in miscarriage, stillbirth, premature birth, and

developmental delays in the newborn. Lead can interfere with the production of red blood cells, leading to anemia [8–10]. Technologies for removing heavy metals from water, such as ion exchange, adsorption, precipitation, and membrane filtration, can be employed to treat contaminated water sources [11–14]. Adsorption is a widely used method for removing heavy metals from water and wastewater. The importance of the adsorption method lies in its efficiency, versatility, cost-effectiveness, and ease of operation, making it a preferred choice for removing heavy metals from water and wastewater in various applications [15,16]. Chitosan-based compounds have a high affinity for heavy metal ions due to their amino and hydroxyl functional groups. These functional groups can interact with heavy metal ions through complexation, leading to their adsorption onto the chitosan surface [17,18]. To overcome mercury pollution, a mesoporous thioacetamide/chitosan (MTA/CS) sorbent was developed by Eissa et al. using a simple method characterized by various techniques and found to efficiently remove Hg(II) ions from liquid solutions with a capacity of 195 mg/g [19]. A cost-effective and reusable chitosan–vermiculite (CSVT) composite was developed by Salih et al. for the selective removal of Cu(II) and Cd(II) ions from aqueous solutions, demonstrating superior adsorption capacities (116.22 mg/g for Cu(II) ions and 147.64 mg/g for Cd(II) ions) due to its enhanced surface area and mesoporosity [20]. Nano-selenium functionalized chitosan gel beads (nanoSe@CBs) were developed by Shao et al. to address the limitations of traditional adsorbents in removing toxic Hg(II) from apple juice, demonstrating a synergy between chitosan and nanoSe for enhanced adsorption efficiency. The adsorbent showed a high uptake capacity of 376.5 mg/g for Hg(II) ions [21]. Wang et al. synthesized novel materials based on nano-FeS and starch or chitosan loaded on peanut shell biochar (PSB). The products demonstrated superior adsorption for Pb(II) ions and nitrogen compounds in wastewater, with maximum capacities reaching 91.74 mg/g and 98.04 mg/g for Pb(II), 16.89 mg/g and 18.45 mg/g for $NO_3$-N, as well as 15.65 mg/g and 18.28 mg/g for $NH_4$-N, for Starch-FeS@PSB and Chitosan-FeS@PSB, respectively. These materials leverage mechanisms like complexation, electrostatic attraction, redox, and physical adsorption for pollutant removal [22]. Zeolites, which are sodium aluminum silicates and sodium metal silicates, are commonly employed in removing heavy metals from water due to their unique properties and adsorption capabilities. One of the primary mechanisms by which zeolites or sodium metal silicates eliminate heavy metal ions involves the process of ion exchange. Heavy metal ions in water are exchanged with cations (e.g., sodium ions) on the surface of the zeolites or sodium metal silicates [23–25]. Novel zeolite adsorbent nanostructures, abbreviated as ED1 and ED2, were developed by Abdelrahman et al. in the absence and presence of novel Gemini cationic surfactants, respectively, for the removal of Pb(II) and Hg(II) ions from water. The maximum removal capacities recorded were 160.77 mg/g and 295.86 mg/g for Pb(II) ions, in addition to 130.89 mg/g and 271.00 mg/g for Hg(II) ions by ED1 and ED2, respectively. These findings indicate that both ED1 and ED2 efficiently remove toxic metals from aqueous solutions with the ion-exchange process [26]. Abdelrahman et al. presented a study on the facile hydrothermal synthesis of sodium manganese silicate hydroxide hydrate/manganese silicate nanocomposite for efficiently removing toxic Pb(II) ions from water by the ion exchange process. They demonstrated that nanocomposites fabricated with and without polyethylene glycol 400, named NF and NP, respectively, showed significant Pb(II) adsorption capacities of 292.39 mg/g for NF and 210.97 mg/g for NP [27].
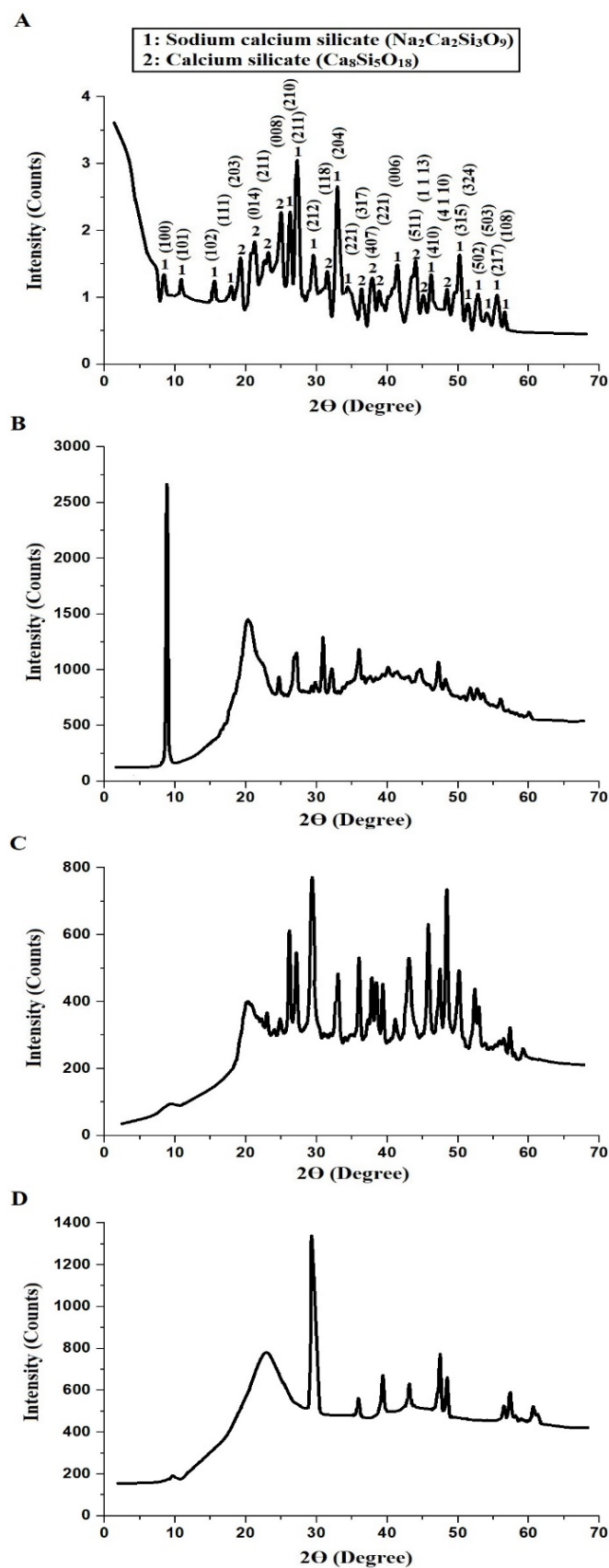
So, in this study, $Na_2Ca_2Si_3O_9$/$Ca_8Si_5O_{18}$ nanostructures (NaCaSilicate) were synthesized and then functionalized via chitosan (CS@NaCaSilicate) and terephthalaldehyde crosslinked chitosan (CCS@NaCaSilicate) as novel nanocomposites for the effective removal of Pb(II) ions. Hence, this research introduces a groundbreaking approach for removing Pb(II) ions from contaminated environments by utilizing nanostructured materials capable of ion exchange processes through sodium ions alongside the natural chelating properties of chitosan or its modified counterparts through complexation with $NH_2$, OH, and C=N groups. Integrating nanostructures that facilitate ion exchange with the complexation abilities of chitosan or its modified counterparts significantly improves the efficiency and

specificity of Pb(II) ion capture. This dual-functionality enhances the selectivity towards Pb(II) ions and offers a reusable and environmentally friendly solution to heavy metal pollution. The research underscores the importance of material science innovation in addressing persistent environmental challenges, highlighting the role of nanotechnology and biopolymers in creating more effective and sustainable solutions for heavy metal removal. Additionally, influences of pH, time, temperature, and preliminary concentration of Pb(II) ions were also considered.
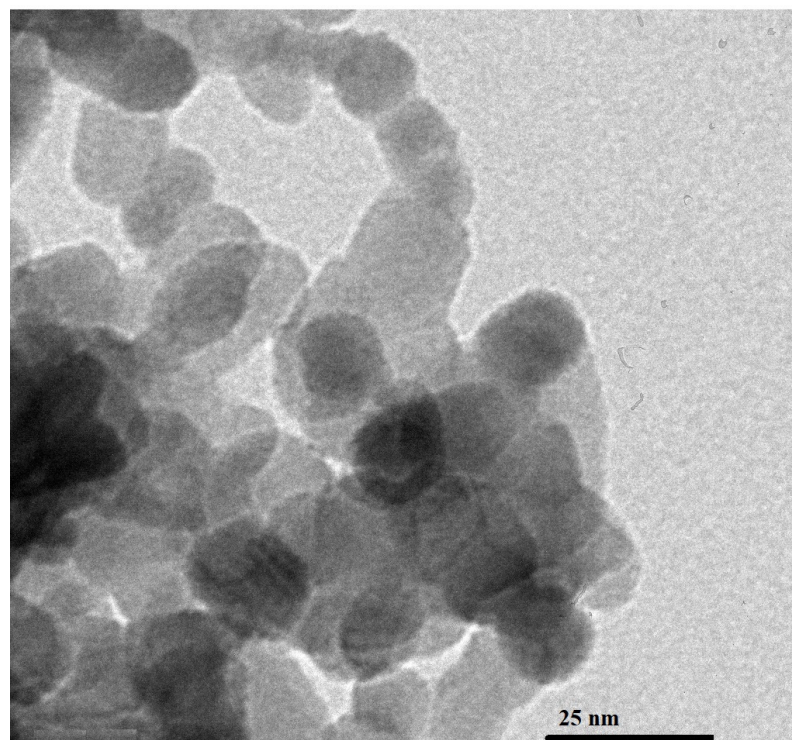
## 2. Results and Discussion

### 2.1. Identification of the Products

Figure 1A–D displays the XRD analysis of the NaCaSilicate, CS, CS@NaCaSilicate, and CCS@NaCaSilicate samples, respectively. Additionally, the findings revealed that the NaCaSilicate sample is composed of sodium calcium silicate ($Na_2Ca_2Si_3O_9$) and calcium silicate ($Ca_8Si_5O_{18}$), as revealed using JCPDS Nos. 00-022-1455 and 00-020-0239, respectively. Additionally, the diffraction peaks at $2\theta$ values of 8.44°, 10.95°, 15.51°, 18.08°, 26.25°, 27.18°, 29.65°, 33.23°, 34.25°, 41.22°, 46.18°, 50.03°, 51.41°, 52.79°, 54.07°, 55.46°, and 56.64° correspond to the (100), (101), (102), (111), (210), (211), (212), (204), (221), (006), (410), (315), (324), (502), (503), (217), and (108) miller indices for $Na_2Ca_2Si_3O_9$, respectively. In addition, the diffraction peaks at $2\theta$ values of 19.09°, 21.11°, 23.13°, 24.79°, 31.58°, 36.45°, 37.82°, 38.83°, 43.69°, 45.17°, and 48.39° correspond to the (203), (014), (211), (008), (118), (317), (407), (221), (511), (1 1 13), and (4 1 10) miller indices for $Ca_8Si_5O_{18}$, respectively. Also, the mean crystal size, as estimated from XRD data, of the NaCaSilicate sample is 13.64 nm. This measurement closely aligns with the estimation derived from HR-TEM, affirming the existence of spheres and polyhedral shapes, each having a mean diameter of 12.92 nm, as illustrated in Figure 2. Also, XRD serves as a potent method for examining the crystallographic structure of substances, encompassing nanoparticles. Variances become apparent when contrasting the XRD patterns of the NaCaSilicate sample with those of the CS@NaCaSilicate and CCS@NaCaSilicate samples. Peak shifts are evident in the XRD patterns of nanostructures that have undergone modification with either chitosan or chitosan crosslinked with terephthalaldehyde, in contrast to the unmodified nanostructures. Such shifts may suggest alterations in the parameters of the crystal lattice, arising from the connection between the NaCaSilicate sample and chitosan or chitosan crosslinked with terephthalaldehyde, as illustrated in Scheme 1. Furthermore, modifications with chitosan or chitosan crosslinked with terephthalaldehyde lead to changes in the intensity of diffraction peaks, indicating modifications in the orientation of the crystal domains and crystallinity within the NaCaSilicate sample. It is essential to highlight that chitosan is mainly identified as an amorphous organic polymer devoid of a distinct and consistent crystal structure during its entirety. Nevertheless, certain peaks at distinct values suggest the presence of localized areas within the chitosan where the chains have been organized in a more structured and crystal-like way.

**Figure 1.** XRD analysis of the NaCaSilicate (**A**), CS (**B**), CS@NaCaSilicate (**C**), and CCS@NaCaSilicate (**D**) samples.
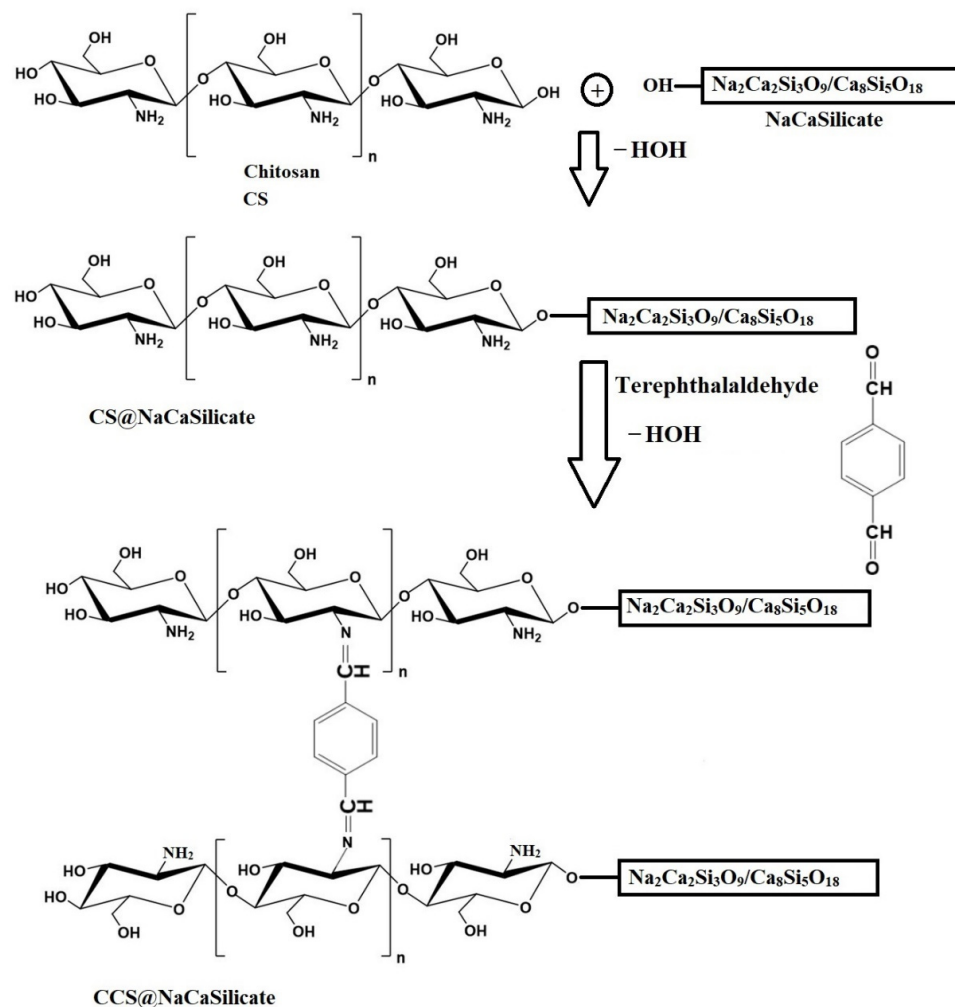
**Figure 2.** HR-TEM analysis of the NaCaSilicate sample.

Figure 3A–C displays the EDS analysis of the NaCaSilicate, CS@NaCaSilicate, and CCS@NaCaSilicate samples, respectively. Also, the results obtained from the EDS data of the NaCaSilicate sample are presented in Table 1, both before and after undergoing modification with chitosan and subsequently with terephthalaldehyde. The elemental composition of the NaCaSilicate sample includes calcium (Ca), silicon (Si), sodium (Na), and oxygen (O). The absence of peaks for other elements confirms the high purity of the NaCaSilicate sample. Following the incorporation of the chitosan with the NaCaSilicate sample, the EDS data reveal the existence of carbon (C) and nitrogen (N). The detection of N and C in the CS@NaCaSilicate sample signifies the effective modification of the NaCaSilicate sample by chitosan. Following the modification of the CS@NaCaSilicate sample with terephthalaldehyde, there is a marked rise in the nitrogen and carbon content as a result of the modification with terephthalaldehyde. Terephthalaldehyde, widely used as a bifunctional cross-linker to enhance the stability and biocompatibility of materials based on chitosan, plays a role in this improvement. The increased levels of nitrogen and carbon in the CCS@NaCaSilicate sample indicate that terephthalaldehyde has crosslinked with chitosan and possibly created extra connections between chitosan and the NaCaSilicate sample.

**Table 1.** EDS analysis of the NaCaSilicate, CS@NaCaSilicate, and CCS@NaCaSilicate products.

| Products | % Si | % Ca | % O | % Na | % C | % N |
|---|---|---|---|---|---|---|
| NaCaSilicate | 19.38 | 13.36 | 63.25 | 4.01 | ---- | ---- |
| CS@NaCaSilicate | 13.89 | 4.86 | 48.39 | 3.84 | 26.26 | 2.76 |
| CCS@NaCaSilicate | 7.94 | 1.05 | 50.73 | 2.96 | 32.54 | 4.78 |

**Scheme 1.** Modification of $Na_2Ca_2Si_3O_9/Ca_8Si_5O_{18}$ nanostructures (NaCaSilicate) via chitosan (CS@NaCaSilicate) and chitosan crosslinked with terephthalaldehyde (CCS@NaCaSilicate).

Figure 4A–D displays the FE-SEM analysis of the NaCaSilicate, CS, CS@NaCaSilicate, and CCS@NaCaSilicate samples, respectively. Prior to any modifications, the NaCaSilicate sample exhibits various morphologies, including polyhedral, rod-like, and irregular shapes. The introduction of chitosan or chitosan crosslinked with terephthalaldehyde induces a significant transformation in the morphology of the NaCaSilicate sample. As a biopolymer, chitosan has the capability to create a layer or coating on the nanostructure surfaces, rendering them more uniform and smoother compared to their unmodified counterparts. Following chitosan modification, there is a potential for more uniform dispersion of the nanostructures. Crosslinking with terephthalaldehyde indicates a denser, more compacted formation within the chitosan framework. This structural change may lead to a decrease in the size and the number of voids and pores in the sample, resulting in a denser and more consolidated form in the FE-SEM image.

Figure 5A–C displays the $N_2$ adsorption-desorption isotherms of the NaCaSilicate, CS@NaCaSilicate, and CCS@NaCaSilicate products. The results show that the resulting curves follow the IV type, confirming their mesoporous nature. Their surface textures, that is, their total pore volume, average pore size, and BET surface area were tabulated in Table 2. The CS@NaCaSilicate and CCS@NaCaSilicate products show a decrease in both total pore volume and BET surface area compared to the NaCaSilicate product due to the modification with chitosan and terephthalaldehyde.

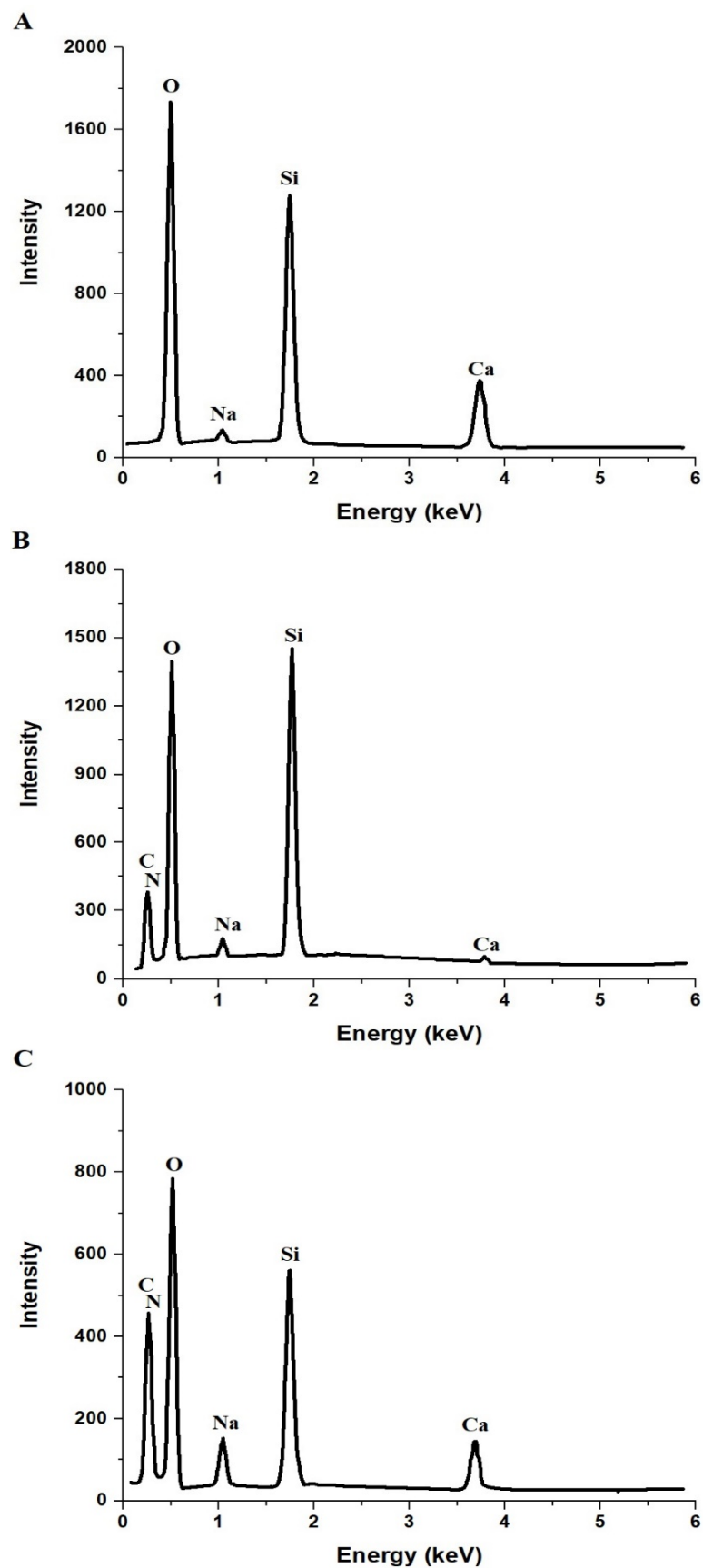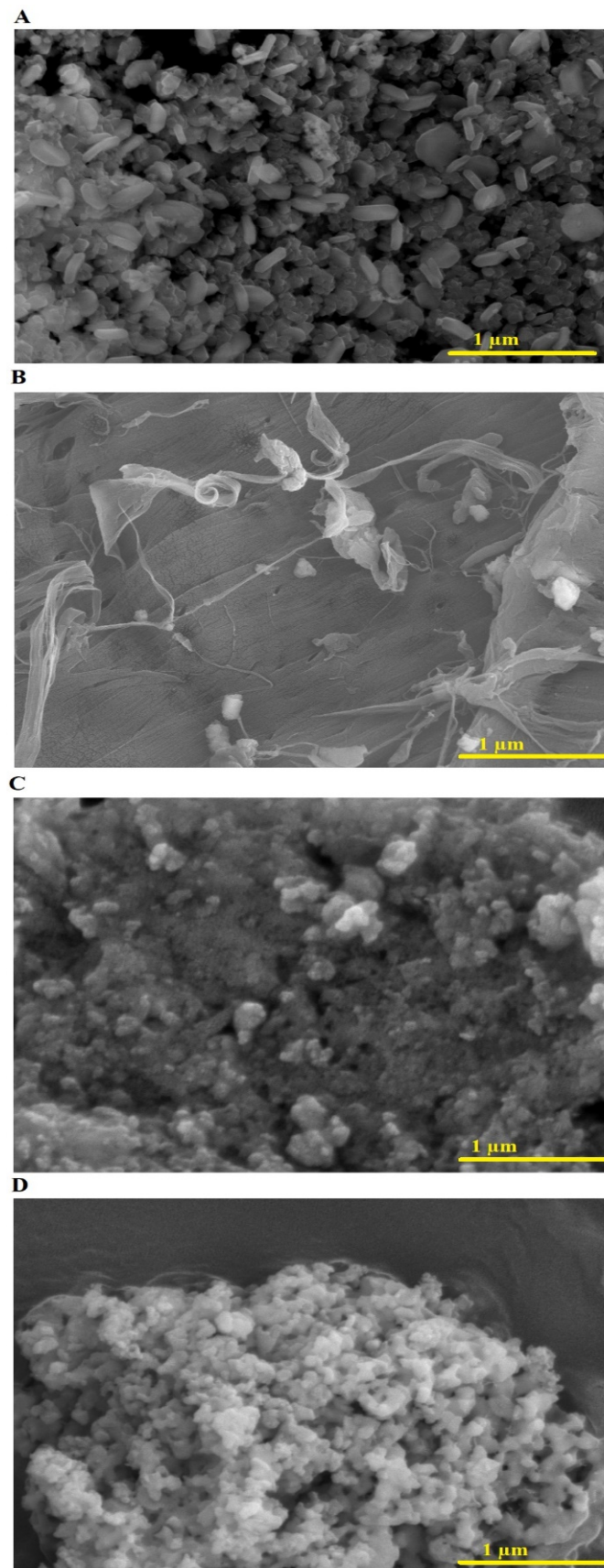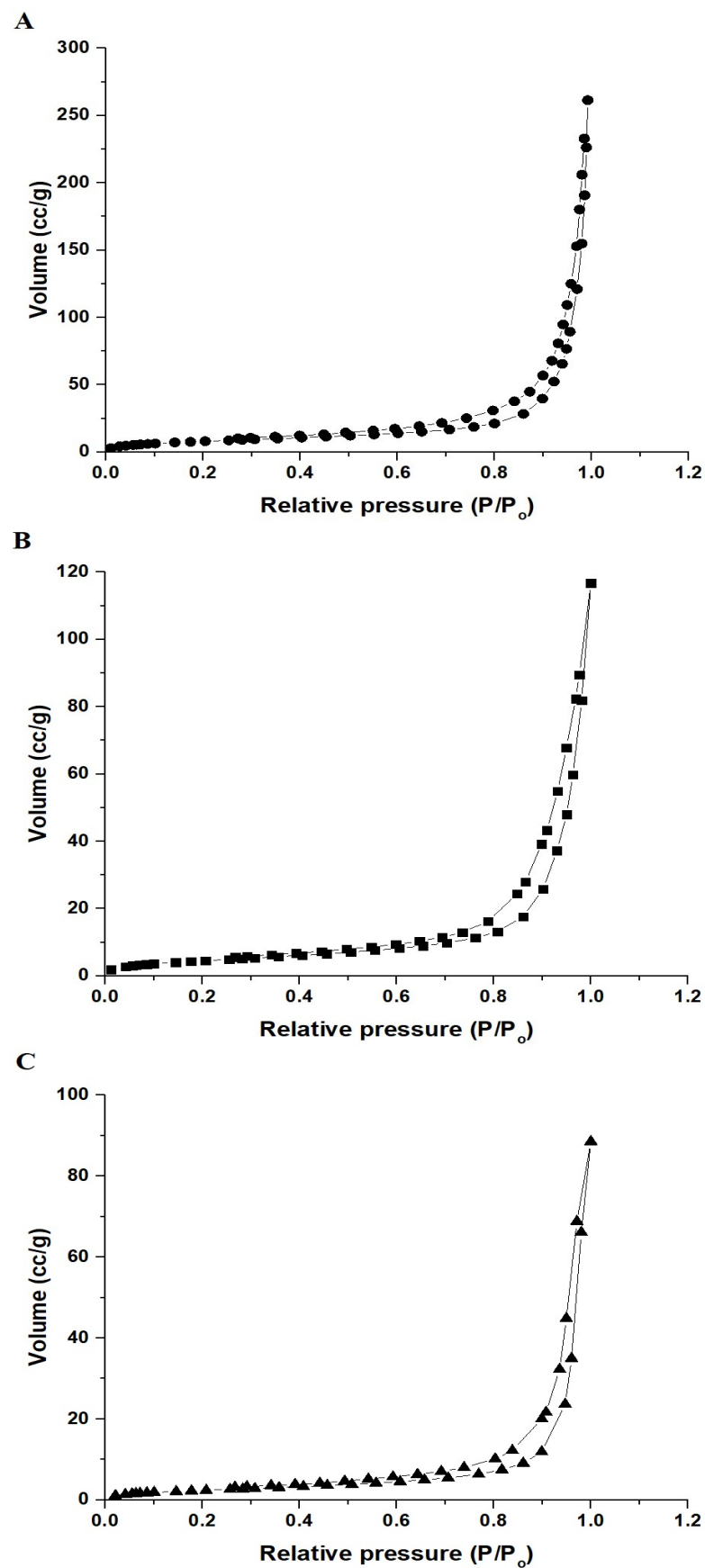**Figure 3.** EDS analysis of the NaCaSilicate (**A**), CS@NaCaSilicate (**B**), and CCS@NaCaSilicate (**C**) samples.

**Figure 4.** FE-SEM analysis of the NaCaSilicate (**A**), CS (**B**), CS@NaCaSilicate (**C**), and CCS@NaCaSilicate (**D**) products.

**Figure 5.** $N_2$ adsorption–desorption isotherms of the NaCaSilicate (**A**), CS@NaCaSilicate (**B**), and CCS@NaCaSilicate (**C**) products.

**Table 2.** Surface textures of the NaCaSilicate, CS@NaCaSilicate, and CCS@NaCaSilicate samples.

| Samples | Total Pore Volume (cc/g) | Average Pore Size (nm) | BET Surface Area (m$^2$/g) |
|---|---|---|---|
| NaCaSilicate | 0.3680 | 48.51 | 30.35 |
| CS@NaCaSilicate | 0.1529 | 35.93 | 17.02 |
| CCS@NaCaSilicate | 0.1199 | 52.25 | 9.18 |

*2.2. Adsorption of Pb(II) Ions from Aqueous Media*

Equation (1) was applied to calculate the elimination percentage of Pb(II) ions (% R), whereas Equation (2) was applied to calculate the adsorption capacity (Q, mg/g) of the fabricated samples [28].
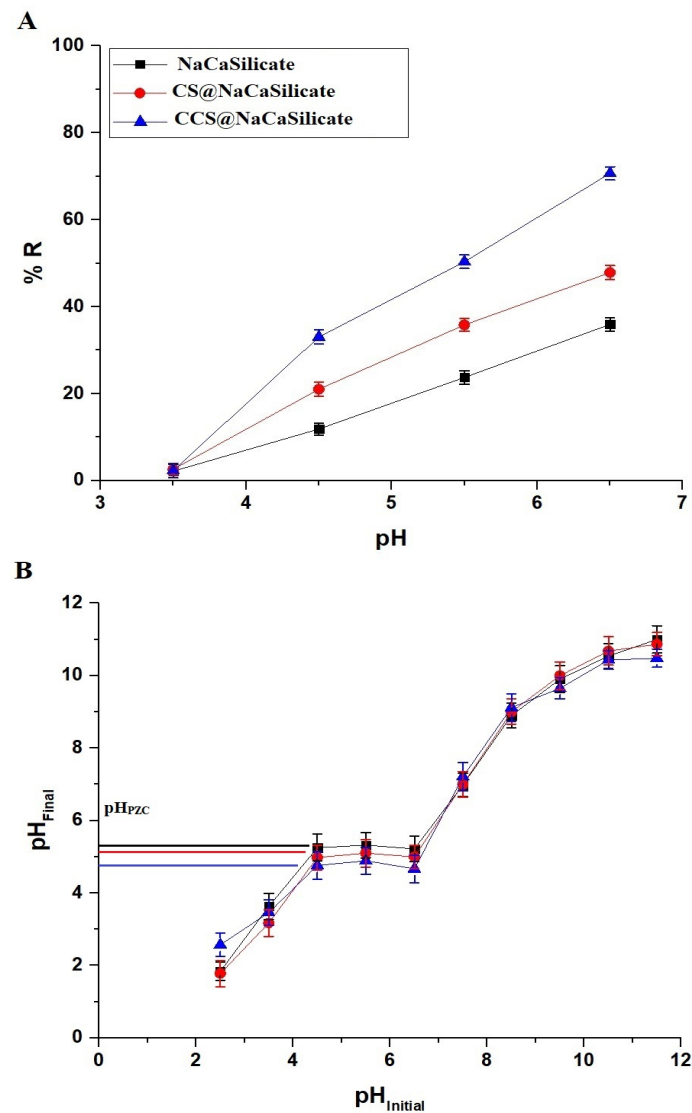
$$\%R = \frac{X_i - X_e}{X_i} \times 100 \tag{1}$$

$$Q = [X_i - X_e] \times \frac{V}{W} \tag{2}$$

where $X_e$ (mg/L) and $X_i$ (mg/L) represent the final and preliminary concentrations of Pb(II) ions, respectively. Additionally, V (L) and W (g) denote the volume of the Pb(II) solution and the mass of the adsorbent, respectively.

2.2.1. Influence of pH

In Figure 6A, the graph shows the change in the elimination percentage of Pb(II) ions concerning the initial pH of the Pb(II) solutions. Also, the point of zero charge (pH$_{PZC}$) for the NaCaSilicate, CS@NaCaSilicate, and CCS@NaCaSilicate samples is determined as 5.25, 5.11, and 4.78, respectively (Figure 6B). Higher removal percentages are associated with pH levels exceeding the pH$_{PZC}$ values. At pH 6.50, the elimination percentages for Pb(II) ions using the NaCaSilicate, CS@NaCaSilicate, and CCS@NaCaSilicate samples are 35.93%, 47.85%, and 70.67%, respectively. Also, in the case of the NaCaSilicate product, elevated pH values compared to pH$_{PZC}$ result in a reduction in the concentration of hydrogen (H$^+$) ions in the solution. Consequently, fewer H$^+$ ions are available to compete with Pb(II) ions for ion exchange sites on the nanostructures, facilitating increased adsorption of Pb(II) ions. The ion exchange positions within the NaCaSilicate sample primarily stem from substitutions and structural defects in the crystal lattice of the NaCaSilicate sample. Some silicon atoms can be replaced by calcium atoms, introducing a net negative charge due to the valence difference. Sodium ions neutralize this charge and can be exchanged with other cations, such as Pb(II) ions. Also, in the case of the CS@NaCaSilicate and CCS@NaCaSilicate samples, the rise in pH beyond pH$_{PZC}$ enhances the number of negatively charged positions (O$^-$ and NH$^-$), resulting from the deprotonation of OH and NH$_2$ groups. This facilitates the elimination of Pb(II) ions through complexation. On the other hand, lower removal efficiencies at pH values below the point of zero charge (pH$_{PZC}$) can be ascribed to electrostatic repulsion between the positively charged Pb(II) ions and the positively charged sites (Na$^+$, OH$_2^+$, and NH$_3^+$) arising from the framework of the NaCaSilicate sample, coupled with the protonation of OH and NH$_2$ groups.

**Figure 6.** Influence of pH on the removal percentage of Pb(II) ions (**A**). Determination of the point of zero charge (pH$_{PZC}$) of the fabricated samples (**B**).
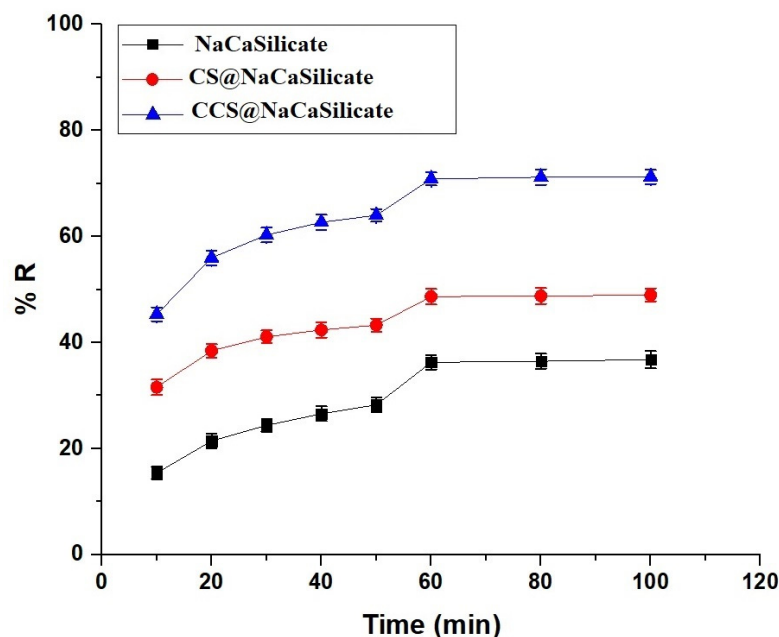
Table 1 represents the EDS analysis of the NaCaSilicate, CS@NaCaSilicate, and CCS@NaCaSilicate products before the adsorption of Pb(II) ions. Additionally, Table 3 represents the EDS analysis of the same products after the adsorption of Pb(II) ions. By comparing the two tables with each other, the presence of lead (Pb) with the disappearance of sodium (Na) and the decrease in the percentage of other elements are evidence of the adsorption of Pb(II) ions into the products by ion exchange and complexation processes.

**Table 3.** EDS analysis of the NaCaSilicate, CS@NaCaSilicate, and CCS@NaCaSilicate products after the adsorption of Pb(II) ions.

| Products | % Si | % Ca | % O | % Na | % C | % N | % Pb |
|---|---|---|---|---|---|---|---|
| NaCaSilicate | 17.01 | 11.72 | 55.48 | ---- | ---- | ---- | 15.79 |
| CS@NaCaSilicate | 11.57 | 4.05 | 40.31 | ---- | 21.87 | 2.29 | 19.91 |
| CCS@NaCaSilicate | 6.12 | 0.80 | 38.21 | ---- | 24.59 | 3.61 | 26.67 |

### 2.2.2. Influence of Contact Time

In Figure 7, the graph depicts the fluctuation in the removal percentage of Pb(II) ions concerning contact time. Also, the efficacy of the fabricated adsorbents is commonly dependent on the contact period of adsorption. A progression in adsorption time from 10 to 60 min correlates with an increase in the removal percentage of adsorbed Pb(II) ions. This augmentation is attributed to the heightened obtainability of free adsorption locations during this duration. On the contrary, the elimination process decelerates with an extension of time from 60 to 100 min as the free adsorption locations become saturated. The elimination percentages of Pb(II) ions using the NaCaSilicate, CS@NaCaSilicate, and CCS@NaCaSilicate samples after 60 min are 36.29, 48.66, and 70.86%, respectively.
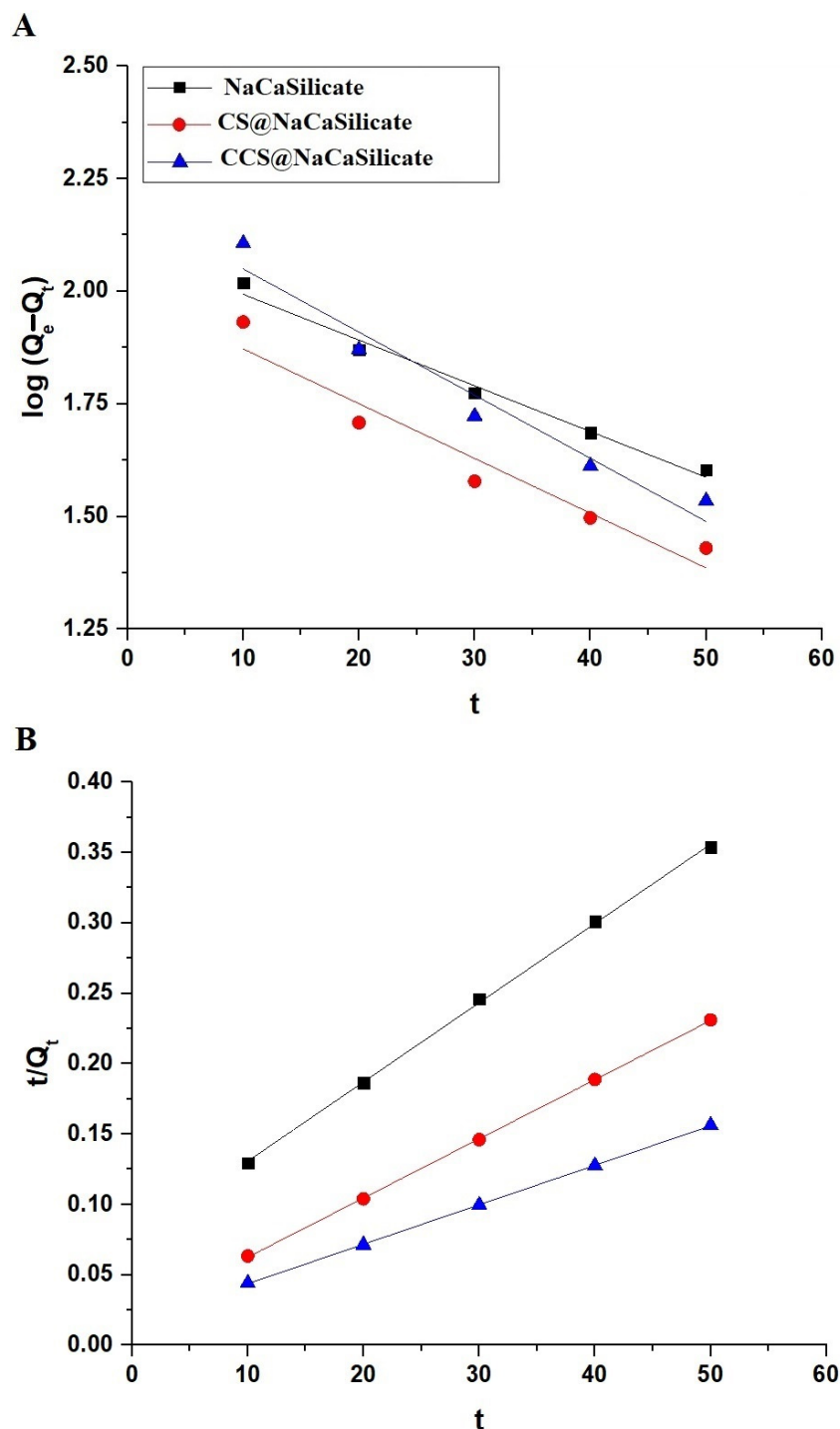


**Figure 7.** Influence of contact time on the removal percentage of Pb(II) ions.

The pseudo-second-order model for adsorption kinetics provides insight into the rate-determining step of the adsorption process, suggesting it is controlled more by the chemisorption mechanism. This model is based on the assumption that the rate of occupation of adsorption sites is proportional to the square of the number of unoccupied sites. The pseudo-first-order model is often applied to systems where physisorption predominates. In the pseudo-first-order model, the rate of adsorption is assumed to be proportional to the number of available sites and is directly related to the difference in saturation concentration and the amount adsorbed at any time [29–33].

Figure 8A,B displays the application of the pseudo-second-order (Equation (3)) and pseudo-first-order (Equation (4)) kinetic models for evaluating the adsorption mechanism of Pb(II) ions onto the surface of the fabricated adsorbents [34,35].

$$\frac{t}{Q_t} = \frac{1}{k_2 Q_e^2} + \frac{1}{Q_e} t \tag{3}$$

$$\log (Q_e - Q_t) = \log Q_e - \frac{k_1}{2.303} t \tag{4}$$

**A**



**B**



**Figure 8.** The plot of the pseudo-first-order (**A**) as well as pseudo-second-order (**B**) models for the elimination of Pb(II) ions using the fabricated samples.

$Q_e$ represents the removal capability of the fabricated samples at equilibrium (mg/g), while $Q_t$ signifies the removal capability of the fabricated samples at contact time t (mg/g). Additionally, $k_1$ denotes the pseudo-first-order rate constant (1/min), and $k_2$ represents the pseudo-second-order rate constant (g/mg·min). Table 4 provides a summary of the kinetic constants. The findings indicate that the elimination of Pb(II) ions by the fabricated adsorbents is most accurately represented by the pseudo-second-order kinetic model, as evidenced by its high correlation coefficient and the close proximity of its adsorption capacity to the practical capacity ($Q_{Exp}$).
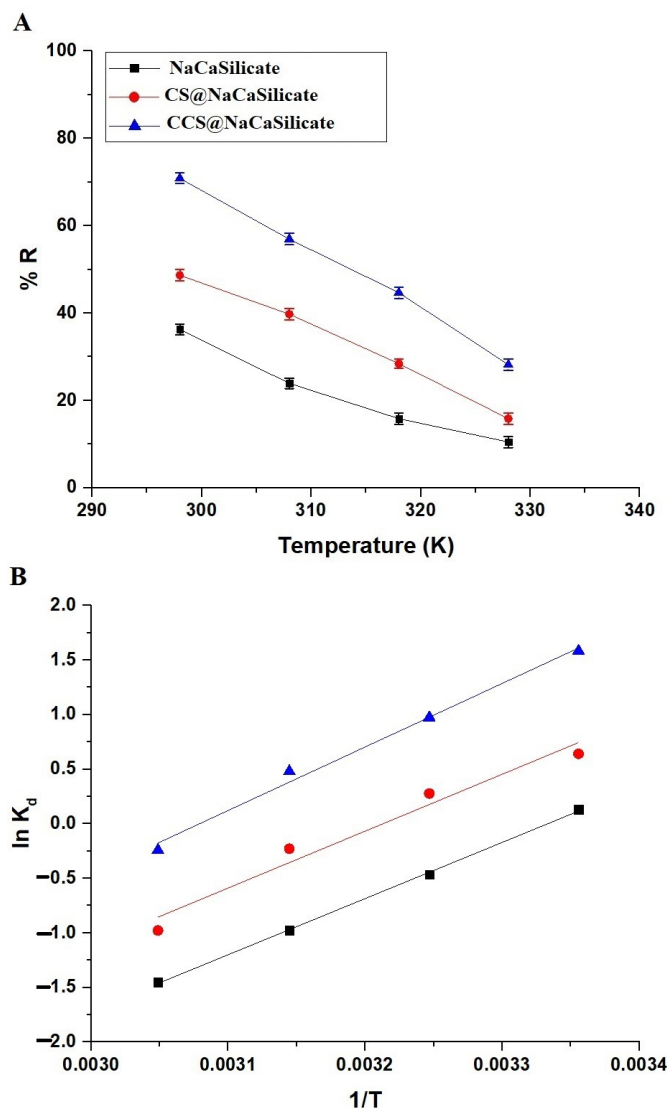
**Table 4.** Kinetic constants for the elimination of Pb(II) ions using the fabricated samples.

| Products | $Q_{Exp}$ (mg/g) | Pseudo-First-Order | | | Pseudo-Second-Order | | |
|---|---|---|---|---|---|---|---|
| | | $Q_e$ (mg/g) | $k_1$ (1/min) | $R^2$ | $Q_e$ (mg/g) | $k_2$ (g/mg.min) | $R^2$ |
| NaCaSilicate | 181.44 | 124.41 | 0.0234 | 0.9796 | 177.62 | 0.0004 | 0.9994 |
| CS@NaCaSilicate | 243.32 | 98.53 | 0.0279 | 0.9157 | 238.09 | 0.0009 | 0.9999 |
| CCS@NaCaSilicate | 354.32 | 154.81 | 0.0323 | 0.9401 | 357.14 | 0.0005 | 0.9999 |

### 2.2.3. Influence of Temperature

In Figure 9A, the graph depicts the change in the removal percentage of Pb(II) ions with respect to the Pb(II) solution temperature. The efficacy of the fabricated adsorbents is commonly affected by the Pb(II) solution temperature. An elevation in Pb(II) solution temperature from 298 to 328 K reduced the elimination percentage of adsorbed Pb(II) ions. As temperature rises, the kinetic energy of Pb(II) ions in solution increases. This heightened movement can reduce interaction time between the Pb(II) ions and the adsorbent surface, as the ions are more likely to bounce off the surface rather than be adsorbed.



**Figure 9.** Influence of temperature on the removal percentage of Pb(II) ions (**A**). The plot of ln $K_d$ versus 1/T (**B**).

In evaluating viability, the assessment encompasses the analysis of thermodynamic constants, including entropy change (ΔS), enthalpy change (ΔH), and free energy (ΔG). These parameters, along with the distribution coefficient ($K_d$) at four different temperatures, are computed employing Equations (5)–(7) [34,35].

$$\ln K_d = \frac{\Delta S}{R} - \frac{\Delta H}{RT} \tag{5}$$

$$K_d = \frac{Q_e}{C_e} \tag{6}$$
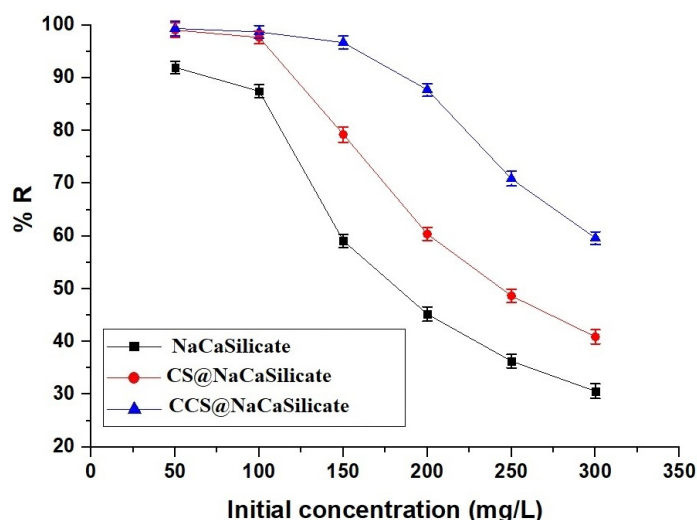
$$\Delta G = \Delta H - T\Delta S \tag{7}$$

T denotes the absolute temperature (in kelvin), while R stands for the universal gas constant (in kJ/mol kelvin). In Figure 9B, the graph illustrates the plot of $\ln K_d$ against $1/T$ for the elimination of Pb(II) ions using the fabricated samples. Also, the thermodynamic constants are compiled in Table 5. The negative values of ΔG for the elimination of Pb(II) ions by the fabricated adsorbents confirm a favorable and spontaneous process. Additionally, the negative values of ΔH indicate exothermic elimination routes. Additionally, the positive values of ΔS indicate a high tendency for Pb(II) ions on the surface of the adsorbent and a larger disorder at the solution/solid boundary. The values of ΔH exceeding 40.00 kJ/mol indicate that the elimination of Pb(II) ions using the fabricated samples occurs through a chemical process.

**Table 5.** Thermodynamic constants for eliminating Pb(II) ions via the fabricated samples.

| Products | ΔH (kJ/mol) | ΔS (kJ/mol kelvin) | ΔG (kJ/mol) | | | |
|---|---|---|---|---|---|---|
| | | | 298 | 308 | 318 | 328 |
| NaCaSilicate | −42.99 | 0.1433 | −85.70 | −87.13 | −88.57 | −89.99 |
| CS@NaCaSilicate | −43.56 | 0.1399 | −85.26 | −86.66 | −88.06 | −89.46 |
| CCS@NaCaSilicate | −48.65 | 0.1498 | −93.29 | −94.79 | −96.29 | −97.79 |

### 2.2.4. Influence of Initial Concentration

Figure 10 depicts the change in the removal percentage of Pb(II) ions in relation to the initial concentration of Pb(II) ions. As the initial concentration of Pb(II) ions rises from 50 to 300 mg/L, there is a decline in the removal percentage of adsorbed Pb(II) ions.
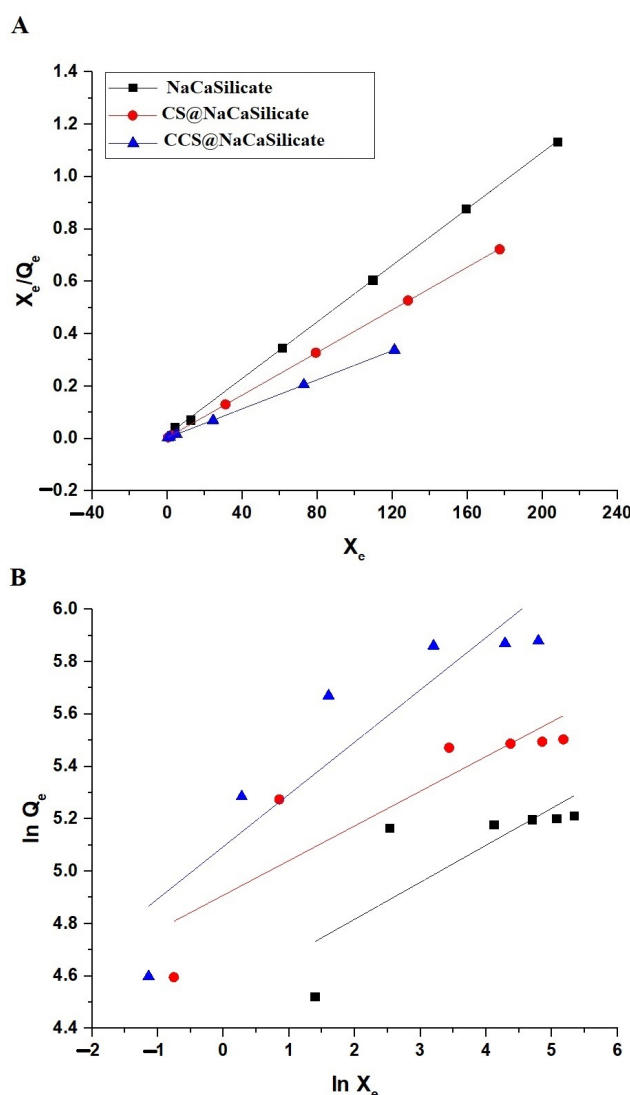


**Figure 10.** Influence of Pb(II) solution temperature on the removal percentage of Pb(II) ions.

The Langmuir adsorption isotherm implies that adsorption occurs on a homogeneous surface via monolayer coverage with no interaction between adsorbed molecules. The Freundlich adsorption isotherm suggests that adsorption occurs on a heterogeneous surface with sites of varying affinities, leading to multilayer adsorption [36].

The elimination mechanism of Pb(II) on the surface of the fabricated samples was evaluated using the Langmuir (Equation (8)) as well as Freundlich (Equation (9)) isotherms, as depicted in Figure 11A,B, respectively [34,35].

$$\frac{X_e}{Q_e} = \frac{1}{k_L Q_m} + \frac{X_e}{Q_m} \tag{8}$$

$$\ln Q_e = \ln k_F + \frac{1}{n}\ln X_e \tag{9}$$



**Figure 11.** The plot of the Langmuir (**A**) as well as Freundlich (**B**) isotherms for the elimination of Pb(II) ions using the fabricated samples.

$Q_m$ (mg/g) denotes the maximum quantity of Pb(II) ions adsorbed per unit mass of adsorbent, while $k_L$ signifies the Langmuir adsorption constant (mg/g). In addition, $k_F$ represents the Freundlich adsorption constant $((mg/g)(L/mg)^{1/n})$, whereas $1/n$ means the heterogeneity constant. Also, Equation (10) was utilized to employ the Freundlich isotherm for determining $Q_m$ [34,35].

$$Q_m = k_F \left( X_i^{1/n} \right) \tag{10}$$

Table 6 provides a summary of the equilibrium constants. The findings indicate that the elimination of Pb(II) ions using the fabricated samples is best described through the Langmuir isotherm, as this applied model's correlation coefficients (R2) are closer to one compared to those of the Freundlich model. The greatest adsorption capability of the NaCaSilicate, CS@NaCaSilicate, and CCS@NaCaSilicate samples for Pb(II) ions is 185.53, 245.70, and 359.71 mg/g, respectively.

**Table 6.** Equilibrium constants for the sorption of Pb(II) ions using the fabricated samples.

| Products | Langmuir | | | Freundlich | | | |
|---|---|---|---|---|---|---|---|
| | $Q_m$ (mg/g) | $k_L$ (L/mg) | $R^2$ | $Q_m$ (mg/g) | $k_F$ (mg/g) $(L/mg)^{1/n}$ | 1/n | $R^2$ |
| NaCaSilicate | 185.53 | 0.3796 | 0.9998 | 203.18 | 93.22 | 0.1411 | 0.5655 |
| CS@NaCaSilicate | 245.70 | 1.0912 | 0.9999 | 281.29 | 135.49 | 0.1323 | 0.7407 |
| CCS@NaCaSilicate | 359.71 | 1.0146 | 0.9999 | 490.63 | 163.12 | 0.1994 | 0.7989 |

Table 7 provides a comparative overview of the performance of the synthesized adsorbents with Pb(II) ions in relation to several previous adsorbents [37–43]. The results of the accomplishment assessment indicate that the fabricated adsorbents displayed exceptional adsorption capacities in comparison to the several adsorbents in the literature.

**Table 7.** Comparison of greatest adsorption capabilities of several adsorbents for the elimination of Pb(II) ions.

| Adsorbents | Adsorption Capacity (mg/g) | Ref. |
|---|---|---|
| Salicylaldehyde/chitosan composite | 123.67 | [37] |
| EGTA/chitosan composite | 106 | [38] |
| Chitosan | 34.98 | [39] |
| Chitosan-iron oxide composite | 214.92 | [40] |
| Graphene oxide/MOF nanohybrid | 254.45 | [41] |
| Mg-Fe layered double hydroxide | 78.73 | [42] |
| Thiol-modified activated carbon | 310.9 | [43] |
| NaCaSilicate | 185.53 | This study |
| CS@NaCaSilicate | 245.70 | This study |
| CCS@NaCaSilicate | 359.71 | This study |

2.2.5. Influence of Desorption and Reusability

Desorption studies were conducted to assess the regenerative and reuse capabilities of the created adsorbents, using 50 mL of several hydrochloric acid concentrations (3, 6, and 9 M) as an eluting agent for Pb(II) ions, as elucidated in Figure 12. In addition, the desorption percentage (% E) of Pb(II) ions from the fabricated adsorbents was computed employing Equation (11) [34,35].

$$\%E = \frac{100X_d V_d}{Q_e W} \tag{11}$$

$V_d$ (L) represents the volume of the HCl eluting agent, while $X_d$ (mg/L) signifies the concentration of Pb(II) ions in the HCl eluting agent. Additionally, the results revealed that a 9 M hydrochloric acid solution efficiently eliminated Pb(II) ions, achieving a desorption efficacy of over 99%.
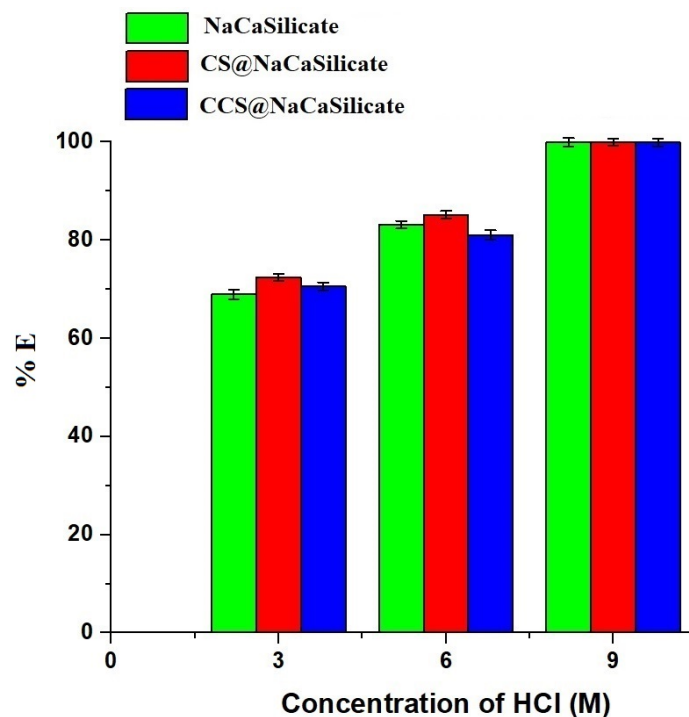
**Figure 12.** Influence of desorption of Pb(II) ions from the fabricated samples.

After the acidic elution process, the regenerated adsorbents underwent rinsing with 250 mL of distilled water to prepare them for subsequent adsorption cycles. Also, the effect of five repeated adsorption/desorption cycles on the elimination of Pb(II) ions was assessed, and the results are shown in Figure 13. The data indicates a slight decrease in the elimination percentage of Pb(II) ions using the fabricated samples with increasing cycle numbers. Therefore, it can be deduced that the fabricated samples demonstrate exceptional reusability activity for the elimination of Pb(II) ions.
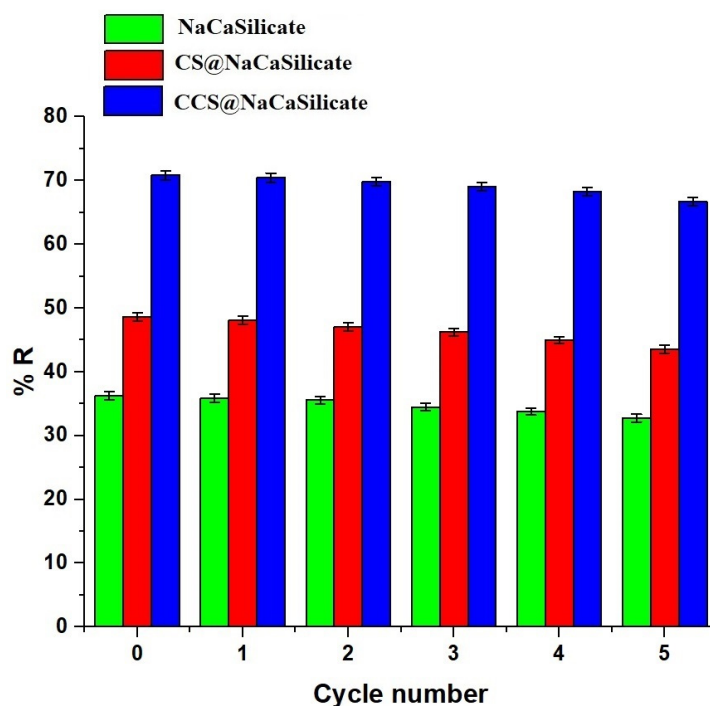


**Figure 13.** Influence of reusability activity of the fabricated samples for the elimination of Pb(II) ions.

## 3. Experimental

### 3.1. Materials

Glacial acetic acid ($CH_3COOH$), calcium chloride dihydrate ($CaCl_2.2H_2O$), chitosan (($C_6H_{11}NO_4)_n$), hydrochloric acid (HCl), sodium metasilicate pentahydrate ($Na_2SiO_3.5H_2O$), terephthalaldehyde ($C_8H_6O_2$), sodium hydroxide (NaOH), lead(II) nitrate ($Pb(NO_3)_2$), and potassium chloride (KCl) were purchased from Sigma-Aldrich company (St. Louis, MO, USA)) and were not further refined.

### 3.2. Fabrication of Adsorbents

#### 3.2.1. Fabrication of $Na_2Ca_2Si_3O_9/Ca_8Si_5O_{18}$ Nanostructures

A silicate solution was prepared by dissolving 15 g of $Na_2SiO_3.5H_2O$ in 100 mL of distilled water. Also, a calcium solution was prepared by dissolving 5 g of $CaCl_2.2H_2O$ in 100 mL of distilled water. Afterward, the calcium solution was added drop by drop through a pipette into the silicate solution, and then the produced mixture was magnetically stirred for 25 min. The formed nanostructures (NaCaSilicate) were separated, thoroughly washed with distilled water, and dried at 60 °C.

#### 3.2.2. Modification of $Na_2Ca_2Si_3O_9/Ca_8Si_5O_{18}$ Nanostructures by Chitosan

A total of 2.5 g of chitosan (CS) was dissolved in an acetic acid mixture (8.5 mL of $CH_3COOH$:130 mL of distilled water) while being continuously stirred magnetically at ambient temperature for 6 h. Subsequently, 2.5 g of NaCaSilicate was charged to the previous CS solution under continuous magnetic stirring at room temperature for 6 h. This mixture was gradually incorporated into the NaOH solution (7.50 g of NaOH:300 mL of distilled water), again under continuous magnetic stirring at room temperature for 6 h. The resultant nanocomposite (CS@NaCaSilicate) was isolated, extensively washed several times with distilled water, and left to dry in the air.

#### 3.2.3. Modification of $Na_2Ca_2Si_3O_9/Ca_8Si_5O_{18}$ Nanostructures via Chitosan Crosslinked with Terephthalaldehyde

2.5 g of chitosan (CS) was dissolved in an acetic acid mixture (8.5 mL of CH3COOH:130 mL of distilled water) while continuously stirred magnetically at ambient temperature for 6 h. Subsequently, 2.5 g of NaCaSilicate was charged to the previous CS solution under continuous magnetic stirring at room temperature for 6 h. A terephthalaldehyde solution (0.5 g of terephthalaldehyde dissolved in 50 mL of methanol) was also charged to the previous solution under continuous magnetic stirring at room temperature for 2 h. Additionally, this mixture was gradually incorporated into the NaOH solution (7.50 g of NaOH: 300 mL of distilled water), again under continuous magnetic stirring at room temperature for 6 h. The resultant nanocomposite (CCS@NaCaSilicate) was isolated, extensively washed several times with distilled water, and left to dry in the air. Scheme 1 shows the modification of nanostructures via chitosan and chitosan crosslinked with terephthalaldehyde. The nanostructures possess OH groups on their surface as a result of the hydrolysis of Ca-OH alongside Si-OH throughout the sol-gel fabrication of these nanostructures.

### 3.3. Instrumentation

X-ray diffraction (XRD) examination of the NaCaSilicate, CS@NaCaSilicate, and CCS@NaCaSilicate samples was performed using an XRD instrument (Bruker D8 Advance, Billerica, MA, USA) operating at a scan rate of 2 degrees per minute, utilizing K$\alpha$ Cu radiation (0.154 nm) at 40 kV. Also, the surface morphologies and elementary composition of the NaCaSilicate, CS@NaCaSilicate, and CCS@NaCaSilicate samples were obtained by a field emission scanning electron microscope/energy dispersive X-ray spectrometer (FE-SEM/EDS, TESCAN, model Vega 3, Brno, Czech Republic) with an operating voltage of 15 kV. Additionally, a high-resolution transmission electron microscope (HR-TEM, Talos F200iS, Hillsboro, OR, USA) was utilized for obtaining the morphology of the NaCaSilicate sample. The surface textures (total pore volume, average pore size, as well as

Brunauer, Emmett, and Teller (BET) surface area) of the NaCaSilicate, CS@NaCaSilicate, and CCS@NaCaSilicate samples were performed using an $N_2$ gas analyzer (Quantachrome, Nova 2000, Graz, Austria).

*3.4. Adsorption of Pb(II) Ions from Aqueous Media*

To conduct the batch elimination experiments, 50 mg of the NaCaSilicate, CS@NaCaSilicate, or CCS@NaCaSilicate adsorbent were introduced into 0.1 L of Pb(II) solutions with varying pH levels (3.5–6.5), each having a concentration of 250 mg/L. Afterward, the mixture of adsorbent and adsorbate underwent 180 min of magnetic stirring, followed by filtration utilizing a centrifuge to isolate the adsorbent. The residual concentration of Pb(II) ions in the filtrate was measured using an atomic absorption spectrophotometer (Shimadzu AA-6300, Kyoto, Japan). Furthermore, additional batch elimination experiments were conducted at pH 6.5 to assess the influence of several impacts, including contact time (10–100 min), elimination temperature (298–328 K), and initial Pb(II) ion concentration (50–300 mg/L). All experiments were repeated twice, and the average was taken into account.

*3.5. Determination of the Point of Zero Charge ($pH_{PZC}$) for the Fabricated Adsorbents*

The determination of the point of zero charge ($pH_{PZC}$) for the fabricated adsorbents followed our prior research methodology [34,35]. In this approach, 100 mg of the NaCaSilicate, CS@NaCaSilicate, or CCS@NaCaSilicate adsorbent were introduced into 0.05 L of KCl solutions that had a chemical concentration of 0.03 M and varied in pH from 2.50 to 11.50. Subsequently, the adsorbents were isolated through centrifugation, and the final pH of the resulting filtrates was measured employing a CYBERSCAN 510 pH meter. Also, a relationship was identified between the preliminary values of pH (displayed on the *x*-axis) and the matching final values of pH (represented on the *y*-axis). The pH final value (on the *y*-axis) determines the zero-charge point, where the resulting curve shows near constancy.

**4. Conclusions**

$Na_2Ca_2Si_3O_9/Ca_8Si_5O_{18}$ nanostructures (NaCaSilicate) were simply synthesized and then successively functionalized with chitosan (CS@NaCaSilicate) and chitosan crosslinked with terephthalaldehyde (CCS@NaCaSilicate). The maximum adsorption capacity of the NaCaSilicate, CS@NaCaSilicate, and CCS@NaCaSilicate samples for Pb(II) ions is 185.53, 245.70, and 359.71 mg/g, respectively. Furthermore, the investigation demonstrated that 9 M HCl effectively eliminated Pb(II) ions from the fabricated samples, attaining a desorption efficacy surpassing 99%. The fabricated samples exhibited exceptional reusability across five successive adsorption/desorption cycles in capturing Pb(II) ions.

**References**

1. Yu, T.; Wang, J.; Ding, N.; Guo, X.; Wang, M.; Chen, Y. Tourmaline for Heavy Metals Removal in Wastewater Treatment : A Review. *J. Ind. Eng. Chem.* **2024**, *131*, 44–53. [CrossRef]
2. Fei, Y.; Hu, Y.H. Recent Progress in Removal of Heavy Metals from Wastewater: A Comprehensive Review. *Chemosphere* **2023**, *335*, 139077. [CrossRef] [PubMed]
3. He, T.; Li, Q.; Lin, T.; Li, J.; Bai, S.; An, S.; Kong, X.; Song, Y.F. Recent Progress on Highly Efficient Removal of Heavy Metals by Layered Double Hydroxides. *Chem. Eng. J.* **2023**, *462*, 142041. [CrossRef]

4.  Di, L.; Chen, X.; Lu, J.; Zhou, Y.; Zhou, Y. Removal of Heavy Metals in Water Using Nano Zero-Valent Iron Composites: A Review. *J. Water Process Eng.* **2023**, *53*, 103913. [CrossRef]

5.  Shamim, M.A.; Zia, H.; Zeeshan, M.; Khan, M.Y.; Shahid, M. Metal Organic Frameworks (MOFs) as a Cutting-Edge Tool for the Selective Detection and Rapid Removal of Heavy Metal Ions from Water: Recent Progress. *J. Environ. Chem. Eng.* **2022**, *10*, 106991. [CrossRef]

6.  Xiang, H.; Min, X.; Tang, C.J.; Sillanpää, M.; Zhao, F. Recent Advances in Membrane Filtration for Heavy Metal Removal from Wastewater: A Mini Review. *J. Water Process Eng.* **2022**, *49*, 103023. [CrossRef]

7.  Abdelwahab, O.; Thabet, W.M. Natural Zeolites and Zeolite Composites for Heavy Metal Removal from Contaminated Water and Their Applications in Aquaculture Systems: A Review. *Egypt. J. Aquat. Res.* **2023**, *49*, 431–443. [CrossRef]

8.  Guo, L.; Zhang, S.F.; Ju, B.Z.; Yang, J.Z.; Quan, X. Removal of Pb(II) from Aqueous Solution by Cross-Linked Starch Phosphate Carbamate. *J. Polym. Res.* **2006**, *13*, 213–217. [CrossRef]

9.  Guo, M.; Chen, H.; Luo, Z.; Lian, Z.; Wei, W. Selective Removal of Pb(II) Ions from Aqueous Solutions by Acrylic Acid/Acrylamide Comonomer Grafted Polypropylene Fibers. *Fibers Polym.* **2017**, *18*, 1459–1467. [CrossRef]

10. Ali, S.M.; El Mansop, M.A.; Galal, A.; El Wahab, S.M.A.; El-Etr, W.M.T.; El-Abdeen, H.A.Z. Removal of Pb(II) Ions by Cellulose Modified-LaFeO$_3$ Sorbents from Different Biomasses. *BMC Chem.* **2023**, *17*, 148. [CrossRef]

11. Kim, J.G.; Ku, J.; Jung, J.; Park, Y.S.; Choi, G.H.; Hwang, S.S.; Lee, J.H.; Lee, A.S. Ion-Exchangeable and Sorptive Reinforced Membranes for Efficient Electrochemical Removal of Heavy Metal Ions in Wastewater. *J. Clean. Prod.* **2024**, *438*, 140779. [CrossRef]

12. Patel, P.K.; Pandey, L.M.; Uppaluri, R.V.S. Highly Effective Removal of Multi-Heavy Metals from Simulated Industrial Effluent through an Adsorption Process Employing Carboxymethyl-Chitosan Composites. *Environ. Res.* **2024**, *240*, 117502. [CrossRef] [PubMed]

13. Chen, Q.; Yao, Y.; Li, X.; Lu, J.; Zhou, J.; Huang, Z. Journal of Water Process Engineering Comparison of Heavy Metal Removals from Aqueous Solutions by Chemical Precipitation and Characteristics of Precipitates. *J. Water Process Eng.* **2018**, *26*, 289–300. [CrossRef]

14. Efome, J.E.; Rana, D.; Matsuura, T.; Lan, C.Q. Effects of Operating Parameters and Coexisting Ions on the Efficiency of Heavy Metal Ions Removal by Nano-Fibrous Metal-Organic Framework Membrane Filtration Process. *Sci. Total Environ.* **2019**, *674*, 355–362. [CrossRef] [PubMed]

15. Küçük, M.E.; Makarava, I.; Kinnarinen, T.; Häkkinen, A. Simultaneous Adsorption of Cu(II), Zn(II), Cd(II) and Pb(II) from Synthetic Wastewater Using NaP and LTA Zeolites Prepared from Biomass Fly Ash. *Heliyon* **2023**, *9*, e20253. [CrossRef] [PubMed]

16. Joseph, I.V.; Tosheva, L.; Doyle, A.M. Simultaneous Removal of Cd(II), Co(II), Cu(II), Pb(II), and Zn(II) Ions from Aqueous Solutions via Adsorption on FAU-Type Zeolites Prepared from Coal Fly Ash. *J. Environ. Chem. Eng.* **2020**, *8*, 103895. [CrossRef]

17. Hassan, S.S.M.; El-Aziz, M.E.A.; Fayez, A.E.S.; Kamel, A.H.; Youssef, A.M. Synthesis and Characterization of Bio-Nanocomposite Based on Chitosan and CaCO$_3$ Nanoparticles for Heavy Metals Removal. *Int. J. Biol. Macromol.* **2024**, *255*, 128007. [CrossRef] [PubMed]

18. Sharifi, M.J.; Nouralishahi, A.; Hallajisani, A. Fe$_3$O$_4$-Chitosan Nanocomposite as a Magnetic Biosorbent for Removal of Nickel and Cobalt Heavy Metals from Polluted Water. *Int. J. Biol. Macromol.* **2023**, *248*, 125984. [CrossRef]

19. Eissa, M.E.; Sakr, A.K.; Hanfi, M.Y.; Sayyed, M.I.; Al-Otaibi, J.S.; Abdel-lateef, A.M.; Cheira, M.F.; Abdelmonem, H.A. Physicochemical Investigation of Mercury Sorption on Mesoporous Thioacetamide/Chitosan from Wastewater. *Chemosphere* **2023**, *341*, 140062. [CrossRef]

20. Salih, S.S.; Shihab, M.A.; Mohammed, H.N.; Kadhom, M.; Albayati, N.; Ghosh, T.K. Chitosan-Vermiculite Composite Adsorbent: Preparation, Characterization, and Competitive Adsorption of Cu(II) and Cd(II) Ions. *J. Water Process Eng.* **2024**, *59*, 105044. [CrossRef]

21. Shao, Z.; Jiang, X.; Lin, Q.; Wu, S.; Zhao, S.; Sun, X.; Cheng, Y.; Fang, Y.; Li, P. Nano-selenium Functionalized Chitosan Gel Beads for Hg(II) Removal from Apple Juice. *Int. J. Biol. Macromol.* **2024**, *261*, 129900. [CrossRef] [PubMed]

22. Wang, H.; Liu, R.; Chen, Q.; Mo, Y.; Zhang, Y. Biochar-Supported Starch/Chitosan-Stabilized Nano-Iron Sulfide Composites for the Removal of Lead Ions and Nitrogen from Aqueous Solutions. *Bioresour. Technol.* **2022**, *347*, 126700. [CrossRef]

23. Zhang, S.; Lv, T.; Mu, Y.; Zheng, J.; Meng, C. High Adsorption of Cd (II) by Modification of Synthetic Zeolites Y, A and Mordenite with Thiourea. *Chin. J. Chem. Eng.* **2020**, *28*, 3117–3125. [CrossRef]

24. Zhang, S.; Cui, M.; Chen, J.; Ding, Z.; Wang, X.; Mu, Y.; Meng, C. Modification of Synthetic Zeolite X by Thiourea and Its Adsorption for Cd (II). *Mater. Lett.* **2019**, *236*, 233–235. [CrossRef]

25. Li, Z.; Wang, L.; Meng, J.; Liu, X.; Xu, J.; Wang, F.; Brookes, P. Zeolite-Supported Nanoscale Zero-Valent Iron: New Findings on Simultaneous Adsorption of Cd(II), Pb(II), and As(III) in Aqueous Solution and Soil. *J. Hazard. Mater.* **2018**, *344*, 1–11. [CrossRef] [PubMed]

26. Abdelrahman, E.A.; El-Dougdoug, W.; Kotp, Y.H. Facile Hydrothermal Synthesis of Novel Zeolite Nanostructures for the Efficient Removal of Pb(II) and Hg(II) Ions from Aqueous Media. *Silicon* **2023**, *15*, 7453–7475. [CrossRef]

27. Abdelrahman, E.A.; Algethami, F.K.; AlSalem, H.S.; Al-Goul, S.T.; Saad, F.A.; El-Sayyad, G.S.; Alghanmi, R.M.; Rehman, K. ur Remarkable Removal of Pb(II) Ions from Aqueous Media Using Facilely Synthesized Sodium Manganese Silicate Hydroxide Hydrate/Manganese Silicate as a Novel Nanocomposite. *J. Inorg. Organomet. Polym. Mater.* **2023**, *34*, 1208–1220. [CrossRef]

28. Pal, D.; Sen, S. Optimal Synthesis of Dolochar Derived Faujasite Zeolite X for Highly Effective Cd(II) Removal. *Environ. Res.* **2024**, *240*, 117494. [CrossRef] [PubMed]

29.    Najafi, F. Removal of Zinc(II) Ion by Graphene Oxide (GO) and Functionalized Graphene Oxide–Glycine (GO–G) as Adsorbents from Aqueous Solution: Kinetics Studies. *Int. Nano Lett.* **2015**, *5*, 171–178. [CrossRef]

30.    He, Z.; Ren, B.; Hursthouse, A.; Wang, Z.A. Efficient Removal of Cd(II) Using $SiO_2$-$Mg(OH)_2$ Nanocomposites Derived from Sepiolite. *Int. J. Environ. Res. Public Health* **2020**, *17*, 2223. [CrossRef]

31.    Ismail, M.; Albadri, A.; Ben Aissa, M.A.; Modwi, A.; Saleh, S.M. High Poisonous Cd Ions Removal by Ru-ZnO-g-C3N4 Nanocomposite: Description and Adsorption Mechanism. *Inorganics* **2023**, *11*, 176. [CrossRef]

32.    Visa, A.; Maranescu, B.; Lupa, L.; Crisan, L.; Borota, A. New Efficient Adsorbent Materials for the Removal of Cd(II) from Aqueous Solutions. *Nanomaterials* **2020**, *10*, 899. [CrossRef] [PubMed]

33.    Wu, Y.; Zhao, Y.; Xu, Z.; Wang, R.; Zhang, H.; Feng, S.; Guo, J. Efficient Removal of Cadmium (II) and Arsenic (V) from Water by the Composite of Iron Manganese Oxides Loaded Muscovite. *Water* **2023**, *15*, 3579. [CrossRef]

34.    Al-wasidi, A.S.; Abdelrahman, E.A. Simple Synthesis and Characterization of Cobalt Ferrite Nanoparticles for the Successful Adsorption of Indigo Carmine Dye from Aqueous Media. *Inorganics* **2023**, *11*, 453. [CrossRef]

35.    Alhalili, Z.; Abdelrahman, E.A. Facile Synthesis and Characterization of Manganese Ferrite Nanoparticles for the Successful Removal of Safranine T Dye from Aqueous Solutions. *Inorganics* **2024**, *12*, 30. [CrossRef]

36.    Velarde, L.; Nikjoo, D.; Escalera, E.; Akhtar, F. Bolivian Natural Zeolite as a Low-Cost Adsorbent for the Adsorption of Cadmium: Isotherms and Kinetics. *Heliyon* **2024**, *10*, e24006. [CrossRef]

37.    Hussain, M.S.; Musharraf, S.G.; Bhanger, M.I.; Malik, M.I. Salicylaldehyde Derivative of Nano-Chitosan as an Efficient Adsorbent for Lead(II), Copper(II), and Cadmium(II) Ions. *Int. J. Biol. Macromol.* **2020**, *147*, 643–652. [CrossRef]

38.    Zhao, F.; Repo, E.; Yin, D.; Sillanpää, M.E.T. Adsorption of Cd(II) and Pb(II) by a Novel EGTA-Modified Chitosan Material: Kinetics and Isotherms. *J. Colloid Interface Sci.* **2013**, *409*, 174–182. [CrossRef] [PubMed]

39.    Ngah, W.S.W.; Fatinathan, S. Pb(II) Biosorption Using Chitosan and Chitosan Derivatives Beads: Equilibrium, Ion Exchange and Mechanism Studies. *J. Environ. Sci.* **2010**, *22*, 338–346. [CrossRef]

40.    Ahmad, R.; Mirza, A. Facile One Pot Green Synthesis of Chitosan-Iron Oxide (CS-$Fe_2O_3$) Nanocomposite: Removal of Pb(II) and Cd(II) from Synthetic and Industrial Wastewater. *J. Clean. Prod.* **2018**, *186*, 342–352. [CrossRef]

41.    Singh, S.; Basavaraju, U.; Kumar, T.S.S.; Kumar, S.; Khan, N.A.; Singh, J.; Singh, L.; Ramamurthy, P.C. Graphene Oxide-Based Novel MOF Nanohybrid for Synergic Removal of Pb (II) Ions from Aqueous Solutions : Simulation and Adsorption Studies. *Environ. Res.* **2023**, *216*, 114750. [CrossRef] [PubMed]

42.    Liang, X.; Hou, W.; Xu, J. Sorption of Pb(II) on mg-Fe Layered Double Hydroxide. *Chin. J. Chem.* **2009**, *27*, 1981–1988. [CrossRef]

43.    Waly, S.M.; El-wakil, A.M.; El-maaty, W.M.A.; Awad, F.S. Efficient Removal of Pb (II) and Hg (II) Ions from Aqueous Solution by Amine and Thiol Modified Activated Carbon. *J. Saudi Chem. Soc.* **2021**, *25*, 101296. [CrossRef]